



HAL
open science

No-Go Decay mRNA cleavage in the ribosome exit tunnel produces 5'-OH ends phosphorylated by Trl1

Albertas Navickas, Sébastien Chamois, Rénette Saint-Fort, Julien Henri,
Claire Torchet, Lionel Benard

► **To cite this version:**

Albertas Navickas, Sébastien Chamois, Rénette Saint-Fort, Julien Henri, Claire Torchet, et al.. No-Go Decay mRNA cleavage in the ribosome exit tunnel produces 5'-OH ends phosphorylated by Trl1. Nature Communications, 2020, 11 (1), pp.122. 10.1038/s41467-019-13991-9 . hal-02495547

HAL Id: hal-02495547

<https://hal.sorbonne-universite.fr/hal-02495547v1>

Submitted on 2 Mar 2020

HAL is a multi-disciplinary open access archive for the deposit and dissemination of scientific research documents, whether they are published or not. The documents may come from teaching and research institutions in France or abroad, or from public or private research centers.





L'archive ouverte pluridisciplinaire **HAL**, est destinée au dépôt et à la diffusion de documents scientifiques de niveau recherche, publiés ou non, émanant des établissements d'enseignement et de recherche français ou étrangers, des laboratoires publics ou privés.

ARTICLE

<https://doi.org/10.1038/s41467-019-13991-9>

OPEN

No-Go Decay mRNA cleavage in the ribosome exit tunnel produces 5'-OH ends phosphorylated by Trl1

Albertas Navickas ^{1,2}, Sébastien Chamois ^{1,2}, Rénette Saint-Fort¹, Julien Henri¹, Claire Torchet ¹ & Lionel Benard ^{1*}

The No-Go Decay (NGD) mRNA surveillance pathway degrades mRNAs containing stacks of stalled ribosomes. Although an endoribonuclease has been proposed to initiate cleavages upstream of the stall sequence, the production of two RNA fragments resulting from a unique cleavage has never been demonstrated. Here we use mRNAs expressing a 3'-ribozyme to produce truncated transcripts *in vivo* to mimic naturally occurring truncated mRNAs known to trigger NGD. This technique allows us to analyse endonucleolytic cleavage events at single-nucleotide resolution starting at the third collided ribosome, which we show to be Hel2-dependent. These cleavages map precisely in the mRNA exit tunnel of the ribosome, 8 nucleotides upstream of the first P-site residue and release 5'-hydroxylated RNA fragments requiring 5'-phosphorylation prior to digestion by the exoribonuclease Xrn1, or alternatively by Dxo1. Finally, we identify the RNA kinase Trl1, alias Rlg1, as an essential player in the degradation of NGD RNAs.

¹Institut de Biologie Physico-Chimique, UMR8226, CNRS, Sorbonne Université, Laboratoire de Biologie moléculaire et Cellulaire des Eucaryotes, Paris, France.

²These authors contributed equally: Albertas Navickas, Sébastien Chamois. *email: lionel.benard@ibpc.fr

The No-Go Decay (NGD) mRNA surveillance pathway degrades mRNAs containing stalled ribosomes^{1,2}. NGD occurs when translation elongation is blocked by the presence of stable intramolecular or intermolecular RNA structures, enzymatic cleavage, chemically damaged sequences or rare codons^{1,3–8}. This mRNA degradation process is dependent on translation and involves an endoribonuclease that cleaves just upstream of the stall sequence^{1,5,6,9}. Other mRNA surveillance pathways can also ultimately lead to NGD. For instance, transcripts synthesized without a stop codon due to premature polyadenylation have stalled ribosomes that are initially detected by the non-stop decay (NSD) pathway^{9,10}. NSD-targeted mRNAs are cleaved by an uncharacterized mechanism and become targets of NGD when ribosomes reach the new 3'-end and stall^{9,11,12}. NGD thus plays a key role in resolving translational issues potentially detrimental to cellular homeostasis. When mRNAs are truncated, the stalled ribosomes are rescued in a process mediated by the Dom34/Hbs1 complex that dissociates the ribosomal subunits⁵. Their association with the 60S subunit is recognized by the ribosome quality control (RQC) pathway, leading to the rapid degradation of the nascent peptide^{13–15}. However, despite extensive study, the precise location of NGD cleavage and the mechanism of degradation of the resulting RNA fragment remain elusive.

In this paper, we focus on the fate of NGD-cleaved mRNAs, with an initial goal of mapping the sites of mRNA cleavage with accuracy. Two major obstacles to achieving this objective are that NGD fragments are rapidly attacked by 5'-3' and 3'-5' exoribonucleases after ribosome dissociation⁵ and that simultaneously blocking the 5'-3' and 3'-5' exoribonuclease decay pathways is synthetically lethal¹⁶. It has been shown, however, that the stability of such mRNAs is largely dependent on the Dom34/Hbs1 complex^{5,17}. In *dom34* mutant cells, ribosomes stalled at the 3'-end of truncated mRNAs inhibit the degradation by the exosome and facilitate the detection of sequential endonucleolytic cleavages upstream of the ribosomal stall site⁵. Interestingly, *dom34* and *xrn1* mutations (inactivating the main 5'-3' exonucleolytic degradation pathway) are not synthetic lethal¹. Moreover, NGD endonucleolytic cleavages still occur in the absence of Dom34^{2,3}. The limited 3'-5' degradation of specific mRNA targets (in the absence of Dom34) combined with 5'-3' exoribonuclease mutants thus allows an accumulation of RNA fragments resulting from endonucleolytic cleavages whose extremities can be mapped accurately. We have created truncated mRNAs in vivo by insertion of a hammerhead ribozyme sequence (Rz)¹⁸ known to generate NGD-targeted mRNAs⁵. This construction mimics chemically or enzymatically cleaved mRNAs, or those resulting from abortively spliced mRNAs that are processed by the NGD pathway^{5,9,19}. As anticipated, these designed truncated 3'-ends block ribosomes at determined positions and, because ribosomes guide NGD mRNA cleavages^{5,20}, we were able to detect 3'-NGD RNA fragments of specific sizes. By analysing these RNAs in detail, we show the importance of the 5'-3' exoribonuclease Xrn1 in the production of 3'-NGD fragments. We also perfectly match a 3'-NGD cleavage product with a 5'-NGD cleavage fragment in the region of the third stalled ribosome. We have mapped this site and show that a unique endonucleolytic cleavage occurs eight nucleotides (nts) upstream of the first P-site nt within the third stacked ribosome. The two leading ribosomes are apparently not competent for this cleavage. We demonstrate that this 3'-NGD RNA has a hydroxylated 5'-extremity and show that 5'-phosphorylation by the Trl1 kinase²¹ is required to allow degradation by 5'-3' exoribonucleases. Interestingly, in the absence of Xrn1, the alternative 5'-3' exoribonuclease Dxo1 takes over²². We additionally analysed mRNAs containing rare codons and demonstrate that at least three stacked ribosomes are also

required for endonucleolytic cleavage of these mRNAs. We show that 5' ends observed in regions covered by disomes are the result of 5'-3' trimming by Dxo1.

Results

Mapping the 5'-ends of 3'-NGD RNA fragments. To generate 3'-truncated mRNA substrates for NGD in vivo, we inserted a hammerhead ribozyme sequence¹⁸ in the 3'-sequence of the *URA3* gene ORF (mRNA1Rz). This results in the production of an mRNA that lacks a stop codon and a polyadenylated tail, called mRNA1 in Fig. 1a and Supplementary Fig. 1a, and that is known to be an NGD target⁵. We first verified that we could detect NGD cleavages in the 3'-proximal region of mRNA1, by northern blotting with a probe corresponding to the 3'-end (probe prA, Fig. 1a and Supplementary Fig. 1a). The upstream and downstream cleavage products are referred to as 5'-NGD and 3'-NGD RNAs, respectively (Fig. 1a). We indeed detected a ladder of 3'-NGD RNA fragments in *dom34* mutant cells (Fig. 1b), in the presence or absence of active 5'-3' or 3'-5' exonucleolytic decay pathways, i.e. *xrn1* or *ski2* mutations, respectively²³. In agreement with the current NGD model in which endonucleolytically cleaved 3'-NGD fragments are primarily degraded by the 5'-3' exoribonuclease Xrn1⁵, inactivation of the 5'-3' RNA decay pathway (*xrn1* mutant cells) produced a different ladder of 3'-NGD RNAs compared to WT or the *ski2* mutant. This was confirmed by a higher resolution PAGE analysis followed by northern blotting (Fig. 1c). The PAGE analysis was completed by mapping the 5'-ends of the 3'-NGD RNA fragments in the *dom34* and *dom34/xrn1* mutants by primer extension experiments with prA (Fig. 1d). We showed that the truncated mRNAs produce several discrete 3'-NGD RNA bands (B1–B5) that can be mapped to single-nucleotide resolution. B5 (77 nts) and the major RNA species B1 (47 nts) visible in the *dom34* mutant were not detected in the absence of the 5'-3' exoribonuclease Xrn1 (Fig. 1b–d). B3 (68 nts) and B2 (65 nts) RNAs were exclusively observed in the *xrn1* mutant cells, and B4 (71 nts) was detected in all four strains (Fig. 1c). In addition, we analysed a *dcp2Δ* decapping mutant that totally blocks 5'-3' exoribonucleolytic attacks on the 5'-end of mRNAs (Fig. 1b, c)^{23,24}. The particularly strong growth defect of the *dcp2Δ* mutant may explain the decrease in the amount of NGD RNA detected but, interestingly, the fact that NGD RNAs remained detectable (Fig. 1c) suggests that an alternative pathway bypasses mRNA decapping for their production.

The sizes of the major B1 and B5 RNAs differ by 30 nts (Fig. 1d), consistent with the length of mRNA covered by an individual ribosome²⁵. We therefore surmised that the difference in size is most likely due to the presence of an extra ribosome protecting the B5 RNA species from 5'-3' degradation by Xrn1, compared to B1²⁶. This prompted us to analyse the association of these 3'-NGD RNAs with ribosomes in sucrose gradients.

Ribosome association with 3'-NGD RNA fragments. We performed polysome analyses to assess the distribution of 3'-NGD RNAs in different ribosomal fractions in *dom34* mutant cells (Fig. 1e, f). The B1 RNA (47 nts) was found to associate with monosomes (fractions 11–13) and disomes (fraction 15), with disomes being the theoretical maximal coverage of such a short RNA, as proposed by Guydosh et al. and Simms et al.^{9,20,27}. Indeed, the association of a 47-nt RNA species with disomes has been deduced from ribosome-profiling experiments²⁰ and is explained by the approximate size of the trailing ribosome protecting a full ribosome footprint (28–30 nt) and the leading ribosome protecting a half footprint to the site of mRNA truncation (16–17 nts, with no RNA or an incomplete codon in the A-site). An additional ribosome would thus be expected to protect a

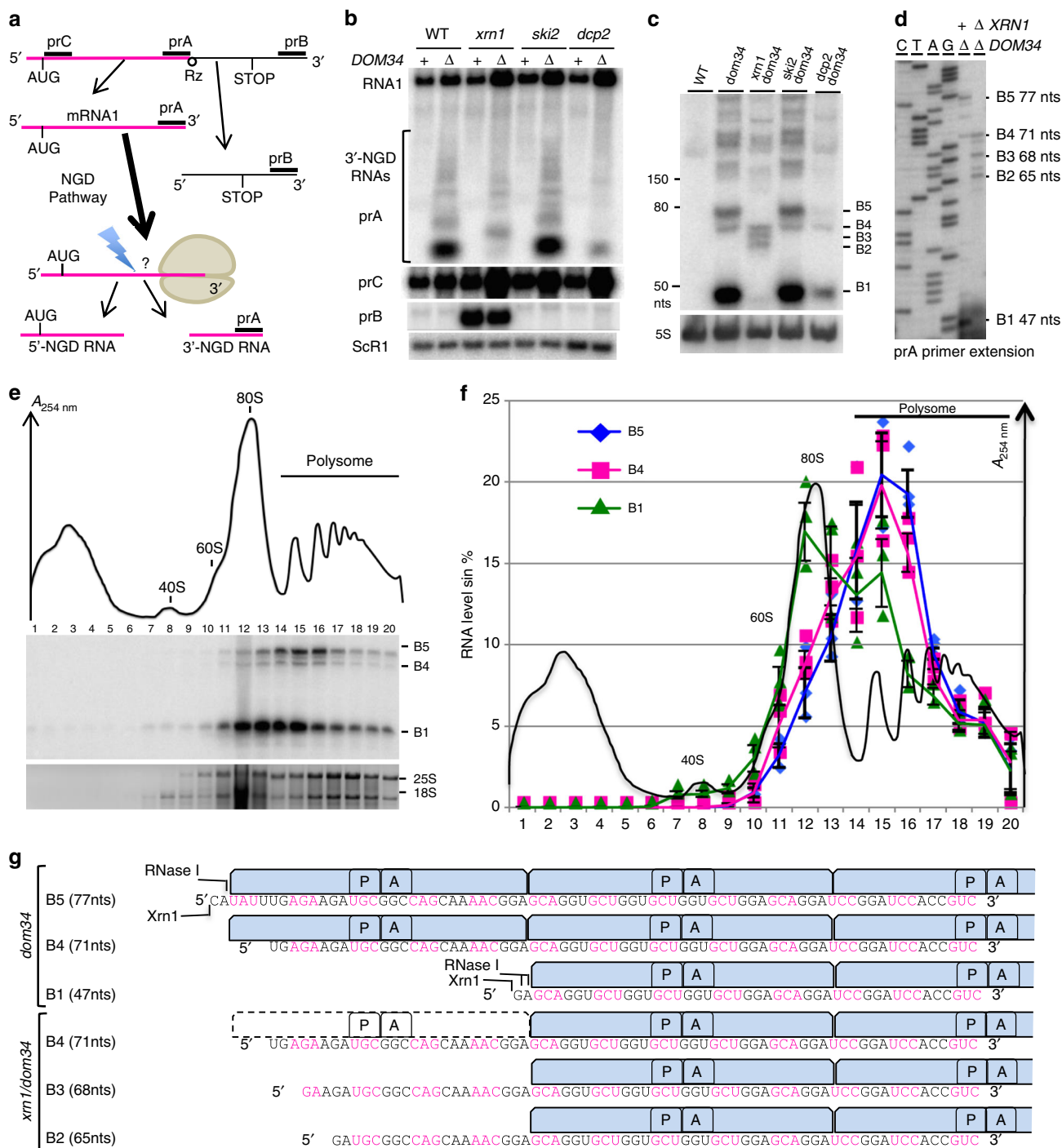


Fig. 1 Size characterization of 3'-NGD RNA fragments and ribosomal association. **a** Schematic view of the URA3Rz mRNA showing the ribozyme (Rz) site (see also Supplementary Fig. 1a). Translational start (AUG) and stop codons are indicated. RNA1 (in magenta) is the stop-codon-less mRNA following ribozyme cleavage. Probes prA, prB and prC used in northern blots analysis are indicated. 5' and 3'-NGD RNAs are the products of NGD cleavage of mRNA1. The lightning flash represents the NGD endonucleolytic cleavage and probe prA is designed for the detection of all potential 3'-NGD RNAs (see also Supplementary Fig. 1a). **b** Agarose gel electrophoresis followed by northern blot showing levels of mRNA1 and 3'-NGD RNA fragments in the indicated strains. The ScR1 RNA served as a loading control. **c** Analysis similar to **b** using 8% PAGE. The 5S rRNA served as a loading control. **d** Primer extension experiments using probe prA to determine the 5'-end of 3'-NGD RNAs. B1, B2, B3, B4 and B5 RNAs shown in **c** are indicated with the corresponding size in nucleotides (nts) calculated by primer extension. **e** Analysis of 3'-NGD RNA association with ribosomes in *dom34* mutant cells. Upper, on ribosome profile, positions of 40S and 60S subunits, 80S and polysome are indicated. Panel below, 20 fractions were collected and extracted RNAs were analysed similarly to **c**. Bottom panel: 18S and 25S rRNAs are shown as references for ribosome and polysome sedimentation, using 1% agarose gel electrophoresis and ethidium bromide staining. **f** Distribution of the 3'-NGD RNAs analysed in **e**. For each fraction, levels of B1, B4 and B5 RNAs were plotted as a % of total amount of B1, B4 and B5 RNAs, respectively. The profile in **e** is reported in **f**. **g** Schematic view of the ribosome positioning on 3'-NGD RNAs combining information on size resolution, ribosomal association (Fig. 1), and RNase ribosomal protection of 3'-NGD RNAs (Supplementary Fig. 1). Codons are shown in black or magenta. A and P are ribosome A- and P-sites, respectively. Error bars indicate standard deviation (s.d.) calculated from three independent experiments. Source data are provided as a Source Data file.

~77-nt RNA. Accordingly, the B5 RNA (77 nts) was found to associate with two and three ribosomes, in fractions 15 and 16, respectively. The 71-nt B4 RNA was also associated with the disome and trisome peaks (Fig. 1e, f). We suspect that ribosomes do not stay stably bound to the different RNA species during sucrose gradient analysis, but this experiment allows us to propose that two ribosomes maximally associate with B1, while up to three can associate with B4 and B5 in vivo. This also prompted us to determine how these 3'-NGD RNAs were protected from Xrn1 and RNase I activities in cell extracts prior to centrifugation on sucrose cushions (Supplementary Fig. 1). These complementary experiments show that ribosomes persist and protect these RNA species from RNases in vitro and support results presented above (Supplementary Notes 1 and 2 and Supplementary Fig. 1b–i).

The results in Fig. 1 and Supplementary Fig. 1 allow us to infer the precise positions of ribosomes on B5 and B4 RNA species in the *dom34* mutant backgrounds. Our experiments all converge to the conclusion that the B5 species corresponds to RNAs covered by trisomes (Fig. 1g). We also conclude that three ribosomes cover the 71-nt B4 RNA in *dom34* mutant cell extracts as this species is resistant to Xrn1 (Supplementary Note 1), its 5'-region is protected from RNase I digestion in vitro (Supplementary Note 2) and a significant proportion remains associated with fractions corresponding to three ribosomes in sucrose gradients (Fig. 1e, f).

Dxo1 trimming of 3'-NGD fragments in Xrn1-deficient cells. We strongly suspected that the B4 species was the original NGD product, and because B3 and B2 RNAs were exclusively detected in Xrn1-deficient cells, we speculated that these RNAs might be derived from B4 by an alternative 5'-3' exoribonuclease. We therefore asked whether the 5'-3' exoribonucleolytic activity of Dxo1, which plays an important role in 5'-end capping quality control²², might explain the presence of the B3 and B2 RNAs. Remarkably, deletion of both *XRN1* and *DXO1* genes in a *dom34* background completely abolished the production of the B3 and B2 RNAs, and only the B4 3'-NGD species remained detectable by northern blot analysis (Fig. 2a) or in primer extension assays (Supplementary Fig. 2a). Complementation of the *dom34/xrn1/*

dxo1 mutant with wild-type Dxo1 restored B3 and B2 RNA production to a significant extent, but a catalytic mutant failed to do so (Fig. 2b). We took advantage of the almost exclusive presence of the B4 3'-NGD RNAs in *dom34/xrn1/dxo1* mutant cells to ask how this RNA is protected by ribosomes by adding Xrn1 to cell extracts as described above (Supplementary Fig. 1b). Some of the B4 RNA was Xrn1-resistant (Supplementary Fig. 2b) in accordance with our hypothesis that a portion of this species is protected by three ribosomes in *xrn1/dom34* cell extracts (Fig. 1g). Interestingly, the decrease in the amount of B4 RNA was correlated with an almost equivalent increase of a 47-nt species (Supplementary Fig. 2b, c), suggesting that disomes persist on the majority of the 3'-ends of B4 RNAs in *dom34/xrn1/dxo1* cells in vivo. We thus propose that two populations of B4 RNAs co-exist in Xrn1-deficient cells in vivo, with one population covered by three ribosomes, especially in *dom34* mutants, and the other only covered by two ribosomes, but having a 5'-protuding RNA extremity due to the absence of 5'-3' exoribonucleases.

Mapping of the primary NGD endonucleolytic cleavage site.

The results described above suggest that the principal band detected in the absence of Xrn1 and Dxo1 (B4 RNA) is a specific 3'-product of NGD cleavage in our constructs (Fig. 2a). While B4 RNA resistance to Xrn1 in vitro (Supplementary Fig. 1b) could be explained by a third ribosome dwelling after cleavage, we also considered the possibility that its 5'-phosphorylation state could contribute to its stability, since both Xrn1 and Dxo1 require 5'-phosphorylated extremities to degrade RNA^{22,28}. We therefore asked whether the B4 RNA naturally has a monophosphate (5'-P) or a hydroxyl group (5'-OH) at its 5'-end by treating RNA purified from *dom34* cell extracts with T4 polynucleotide kinase to see whether this would stimulate attack of B4 by Xrn1 in vitro. Remarkably, the B4 RNA was completely degraded by Xrn1 only after 5'-phosphorylation by T4 kinase in vitro (Fig. 3a), demonstrating that the B4 RNA has a 5'-OH extremity in *dom34* cells. A portion of the abundant B1 RNA persisted during Xrn1 treatment in kinase buffer (Fig. 3a, and see the "Methods" section), but parallel Xrn1 digestion in optimal buffer confirms that B1 and B5 RNAs were totally digested (i.e., are fully mono-phosphorylated), while the B4 RNA remained resistant (Supplementary Fig. 3a). It has recently been demonstrated that the Hel2 ubiquitin-protein ligase is crucial for the activation of NGD cleavages²⁹. Consistent with our hypothesis that the B4 species corresponds to the 3' NGD cleavage product, this RNA is no longer produced in the *hel2* mutant (Supplementary Fig. 3b).

By definition endonucleolytic cleavage of RNA results in the production of 5' and 3'-RNA fragments. However, corresponding 5' and 3' fragments have never been definitively demonstrated in the case of NGD-targeted mRNAs. We thus searched for the corresponding 5'-NGD fragment for the B4 3'-NGD RNA. To map the 3'-end of 5'-NGD RNAs, total RNA preparations from *ski2* and *ski2/dom34* mutants were ligated to a pre-adenylated oligonucleotide linker using truncated RNA ligase to perform 3'-RACE (Fig. 3b)^{30,31}. The *ski2* mutant context was used to limit 3'-trimming of these RNAs in vivo, and RNAs were pre-treated with T4 polynucleotide kinase to modify 3' phosphates or 2'-3' cyclic phosphates to 3'-OH to permit RNA ligation³¹. The major RT-PCR product was of the expected size (66 bp; Fig. 3c and Supplementary Fig. 3c) and verified by sequencing the resulting clones (Fig. 3d). The identification of a matching 5'-NGD fragment for the B4 3'-NGD RNA, confirms that an endonucleolytic event occurred at this precise position. The same procedure performed on RNAs isolated from *ski2* mutants where Dom34 was still active yielded the same major PCR product, also verified by sequencing (Supplementary Fig. 3d). Thus, while the

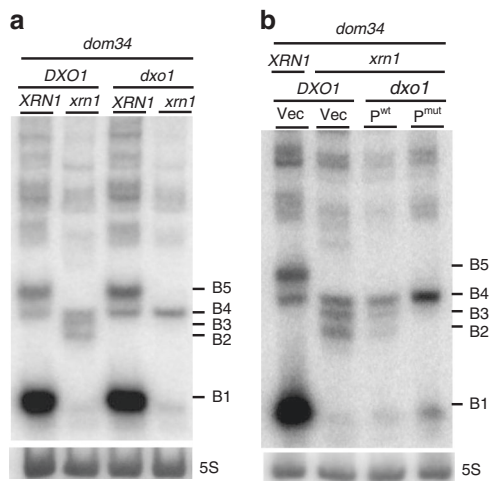


Fig. 2 Dxo1 creates the heterogeneity of 3'-NGD RNA fragments in Xrn1-deficient cells. 8% PAGE followed by northern blot analysis using probe prA showing steady-state levels of RNAs in *dom34* and other indicated mutant strains. The 5S rRNA served as a loading control. **a** Impact of *DXO1* deletion on B2 and B3 RNA production. **b** Plasmid expression of wild-type Dxo1 (P^{wt}) or a Dxo1 catalytic mutant (P^{mut}) (mutant E260A/D262A)²². The vector control is plasmid pRS313 (Vec). Source data are provided as a Source Data file.

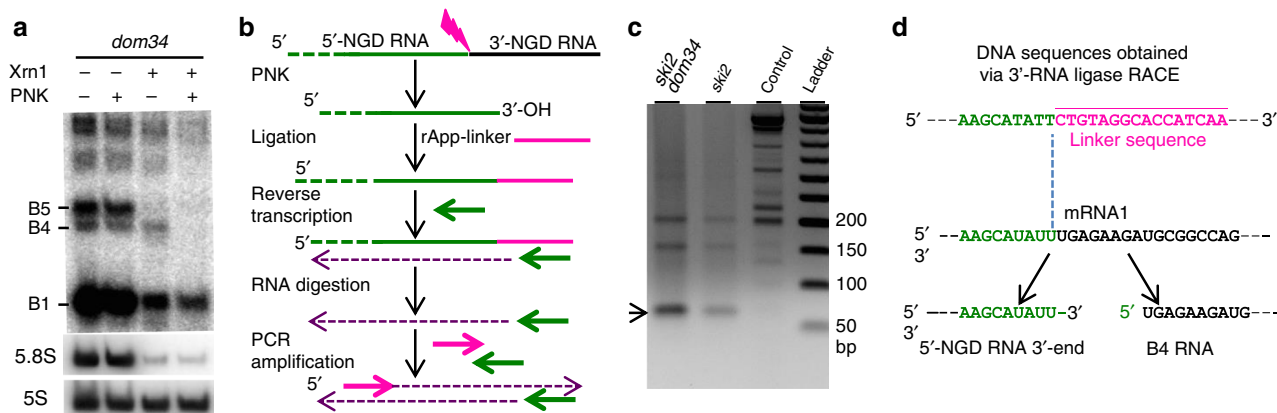


Fig. 3 Characterization of the endonucleolytic RNA fragments. **a** Xrn1 digestion of total RNA extracts from *dom34* mutant cells in the presence or absence of polynucleotide kinase (PNK) in vitro. 8% PAGE followed by northern blot analysis using probe prA. The 5S rRNA served as a loading control and 5.8S rRNA as a positive control of Xrn1 treatment. **b** Flow chart illustrating the method used for 3'-RACE as described in ref. ³¹ with minor modifications according to McGlincy and Ingolia³⁰ (see the Methods section). **c** PCR products obtained from 3'-RACE and separated on a 2% agarose gel. Purified DNAs for sequencing are indicated by an arrowhead. Prior to PCR, cDNAs were produced from total RNA from *ski2*, *ski2/dom34* mutant cells expressing mRNA1. Control is made of total RNA from *ski2/dom34* mutant cells without mRNA1 expression. **d** Sequences obtained after 3'-RACE performed on *ski2* and *ski2/dom34* total RNA. 100% of sequenced clones (omitting a residual 5S rRNA-linker amplification detected) have this DNA sequence. 5'-NGD DNA sequence (in green) and linker sequence (in magenta). Below, the site of mRNA1 is shown before and after the cleavage producing the 3'-NGD RNA B4 and the 3'-extremity of the 5'-NGD RNA confirmed by 3'-RACE. Source data are provided as a Source Data file.

dom34 mutation facilitates the detection of NGD fragments by increasing their stability, the cleavage event itself is Dom34-independent.

The fate of 5'-NGD RNAs. We anticipated that following NGD cleavage of mRNA1, ribosomes that had initiated translation on the 5'-NGD fragments would advance to the new 3'-end and the RNA be subjected to Xrn1 trimming, similar to the process that generates B1 and B5 (Fig. 4a). Since the B4 3'-NGD RNAs were cut in the +1 reading frame (Fig. 1g), upstream ribosomes on these 5'-NGD RNAs would be expected to stall with one nucleotide in ribosome A-site (Fig. 4a and Supplementary Fig. 4) and as result produce new RNA fragments 47 + 1, 77 + 1 nts, protected by two or three ribosomes, respectively (see Supplementary Fig. 4). Indeed, in northern blots using probe prG, which is complementary to the new 3'-ends generated by NGD cleavage, we detected RNA fragments consistent with a 1-nt increase in size compared to those detected by prA on the same membrane (Fig. 4b). We mapped the 5'-ends of these new ribosome protected fragments by primer extension assays using prG (Fig. 4c and Supplementary Fig. 4). The detection of 48-nt (and 78-nt) cDNAs only in cells containing active Xrn1 (Fig. 4c) strongly suggests that the new NGD endonucleolytic products are covered by two and three ribosomes, respectively. The production of cDNAs of exactly the predicted sizes (48 and 78 nts) is an independent confirmation that the 3'-extremity of the 5'-NGD product corresponds precisely to the proposed NGD endonucleolytic cleavage site (Supplementary Fig. 4). Remarkably, the 3'-extremity of the 5'-NGD RNA was detected in the context of active 3'-5' exonucleases, meaning that ribosomes run on and cover the 3'-extremity before any 3'-5' attacks can occur. In summary, we propose that the B4 RNA is produced by endonucleolytic cleavage within the footprint of the third stalled ribosome and that at least two upstream ribosomes promptly protect the resulting 5'-NGD fragment from degradation by 3'-5' exoribonucleases (Fig. 4d).

The 5'-OH endocleaved product is phosphorylated by Trl1. Despite the fact that a portion of the B4 species was found to be 5'-hydroxylated in *dom34* cell extracts (Fig. 3a), a major fraction

of the B4 RNA from *dom34/xrn1* and *dom34/xrn1/dxo1* cell extracts can be degraded by Xrn1 in vitro without prior 5'-phosphorylation (Supplementary Figs. 1b and 2b), suggesting that B4 accumulates as a 5'-phosphorylated species in this mutant background. A well-characterized factor with RNA kinase activity in yeast is the essential tRNA ligase Trl1^{21,32}. Splicing of tRNAs is known to generate 5'-OH-intron RNAs which require Trl1 kinase activity to permit their degradation by Xrn1. We therefore asked whether the 3'-NGD B4 RNA fragments were substrates of Trl1. Since *TRL1* is an essential gene, we used *trl1Δ* strains expressing pre-spliced intron-less versions of the 10 intron-containing tRNAs that restore viability^{33,34}. If Trl1 were required for B4 degradation, loss of Trl1 function should increase the amount of B4 RNA. Remarkably, in *trl1* versus *TRL1* cells, we observed a 24-fold accumulation of the B4 RNA species and only a two-fold-decrease of B1 RNA levels, while the B5 RNA was barely detectable (Fig. 5a, b). We asked whether the accumulated B4 RNA had a hydroxyl group (5'-OH) at its 5'-end. RNAs were analysed by 12% PAGE allowing separation of 5'-hydroxylated from 5'-phosphorylated RNAs²¹. B4 RNA migrated as two bands in *TRL1* cells, whereas only the lower band was detected in *trl1Δ* cells. This species was fully shifted to the upper band after 5'-phosphorylation of RNA in vitro (Fig. 5c). We also verified that the B4 RNA was resistant to Xrn1 treatment in vitro. In contrast to B1 and B5 RNAs (Supplementary Fig. 5), B4 was completely degraded by Xrn1 only after 5'-phosphorylation by T4 kinase in vitro (Fig. 5d). We conclude that the B4 RNA accumulates as a fully 5'-OH species in the *trl1Δ* mutant. Thus, Trl1 is the major kinase involved in phosphorylating the B4 RNA following NGD cleavage.

NGD cleavage products derived from mRNAs containing rare codons. We asked whether we could identify endonucleolytic cleavages on another NGD-targeted mRNAs, using what we learned about this process on truncated mRNAs. We chose an mRNA containing four contiguous rare CGA codons, which we call (CGA)₄-mRNA, as an NGD target (Fig. 6a and Supplementary Fig. 6a)⁵. Similar to the truncated mRNAs, ribosomes were shown to stall when decoding rare codons, producing 5'- and 3'-NGD RNAs (Fig. 6a). As previously demonstrated^{5,35},

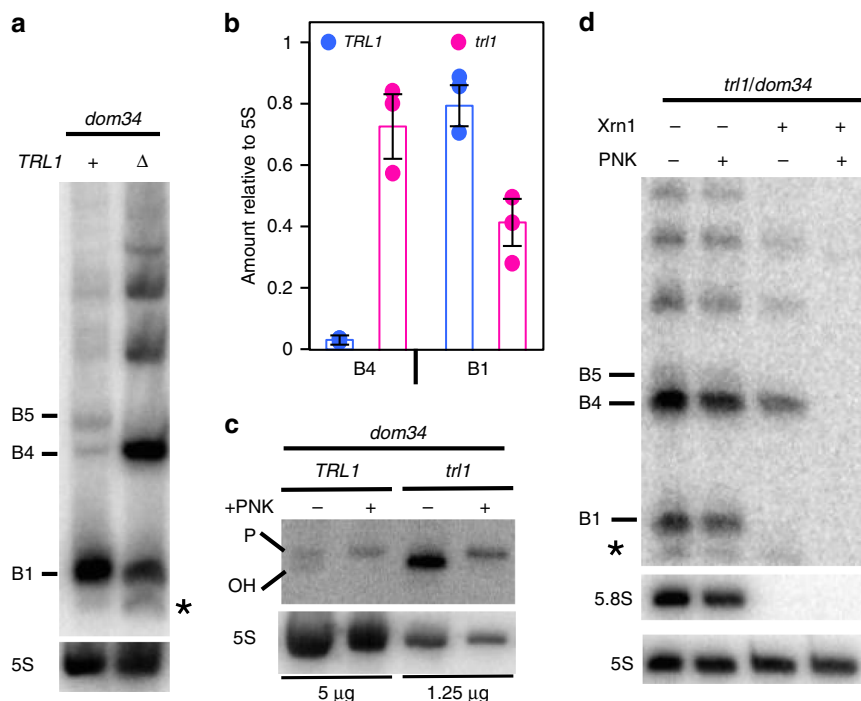


Fig. 5 Endonucleolytically cleaved 5'-OH RNAs are phosphorylated by Trl1. **a** 8% PAGE followed by northern blot analysis using probe prA. Levels of 3'-NGD RNA fragments in *trl1/dom34* cells compared with those from *TRL1/dom34* cells. **b** B1 and B4 RNA quantification relative to 5S rRNA from three independent experiments as shown in **a**. **c** 12% PAGE followed by northern blot analysis using probe prA. Treatment using T4 PNK to determine 5'-OH and 5'-P B4 RNA positions in the indicated strains. One-fourth of *trl1/dom34* total RNA treated was loaded to limit scan saturation and allow *TRL1/dom34* B4 RNA detection. The 5S rRNA served as a loading control. **d** As in Fig. 3a, Xrn1 digestion of total RNA extracts from *trl1/dom34* mutant cells in the presence or absence of T4 PNK treatment in vitro. A minor band detected in *trl1* is indicated by an asterisk (see also Supplementary Fig. 5 in which this band is detectable in *TRL1* cells). Error bars indicate standard deviation (s.d.) calculated from three independent experiments. Source data are provided as a Source Data file.

truncated mRNAs. All these results taken together suggest that the (CGA)₄-mRNA and truncated mRNA1 are NGD-targeted in a highly similar process that results in cleavage within the footprint of the third ribosome, 71 nts upstream of the stall site for the leading ribosome.

Cleavages have been proposed by others to occur in the region covered by disomes using primer extension experiments^{5,29}. We thus analysed an mRNA containing rare codons with an identical ribosome stalling sequence to that previously examined⁵ (Supplementary Fig. 6e). We demonstrate that primer extension arrests detected in the region covered by disomes are abolished in *dxo1/xrn1* mutant cells, suggesting that they are the products of subsequent trimming by these enzymes. In conclusion, our data suggests that stalled disomes on truncated mRNAs or on mRNAs containing short CGA repeats are poorly competent for NGD endonucleolytic cleavages. Endonucleolytic cleavages instead occur upstream of collided disomes, in agreement with other 3'-RACE analyses²⁷. Our data suggests that these cleavages first occur within the mRNA exit tunnel of the third stacked ribosome and those queuing further upstream.

Discussion

In this study, we first characterized the 3'-NGD RNA fragments produced near the 3'-end of truncated mRNAs that mimic natural cleaved mRNAs known to be NGD targets. One advantage of studying the 3'-NGD products of truncated mRNAs is that the precise positioning of stalled ribosomes results in 3'-NGD RNA fragments of specific sizes. Indeed, the precise identification of endonucleolytic cleavages is known to be challenging for mRNAs containing rare codons^{5,29} because the positioning of ribosomes on multiple contiguous rare codons is variable. Using a ribozyme

to efficiently generate precise 3'-ends within an open-reading frame, we were able to obtain detailed information about ribosome positioning on 3'-NGD RNAs, and provide the first precise mapping of the original site of endonucleolytic cleavage on an NGD substrate. Our model suggests that this cleavage occurs 71 nts from the 3' end of the truncated mRNA, 8 nts upstream of the P-site codon in the third stacked ribosome (Figs. 1g and 7). This localizes the 5'-extremity of cleaved RNA fragment within the mRNA exit tunnel, 4 nts downstream of the expected nucleotide position of a canonical mRNA that emerges from the ribosome and becomes available for cleavage by RNase I in vitro, classically used in ribosome foot-printing studies. A buried cleavage site is consistent with the idea that the NGD endonuclease might be the ribosome itself. However, we cannot fully exclude the possibility that the stalled ribosome allows access to an external nuclease with a specific conformation to penetrate this far into the mRNA exit tunnel.

Xrn1 treatment of various mutant cell extracts suggested that the predominant ribosome configuration on truncated mRNAs is disomes. Interestingly, the existence of disomes on truncated mRNAs has been previously reported in ribosome-profiling analysis²⁰ and stacking of two or more ribosomes has been proposed as a prerequisite for the activation of the endonuclease²⁷. The latter observation led to the proposition that ribosome collision triggers NGD cleavage upstream of disomes. Our data suggests that NGD endonucleolytic cleavage detected within the third stalled ribosome, suggests that the first two stalled ribosomes (disome) are not competent for the activation of the endonuclease activity (Fig. 7). Our 3'-RACE experiments did not amplify DNA products corresponding to RNAs matching the predicted sizes of NGD-cleaved RNAs within the second (41 nts) or first stalled ribosome (15 nts) (predicted sizes 95 and 125

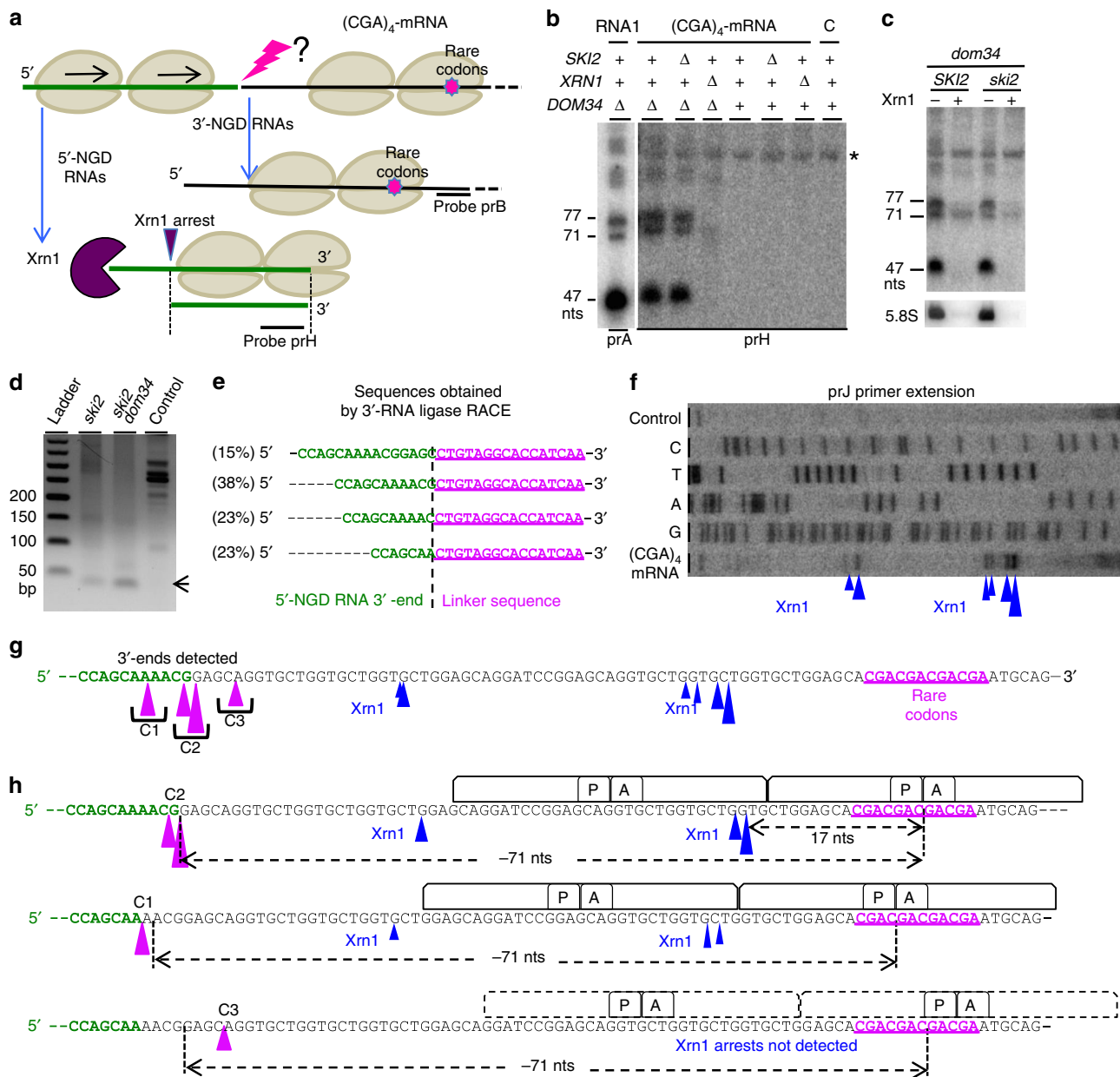


Fig. 6 Identification of the endonucleolytic cuts on the NGD targeted $(CGA)_4$ -mRNA. **a** Schematic view of the $(CGA)_4$ -mRNA. 5'- and 3'-NGD RNAs are products of NGD. The lightning flash represents the potential endonucleolytic cleavage upstream of the ribosome stall site. Probes prB and prH are indicated. 5'-NDG RNAs are shown processed by Xrn1 as described in Figs. 4a, d and Supplementary Fig. 4. **b** Northern blot analysis using probe prH showing steady-state levels of RNAs in the indicated mutant strains. Same membrane has been probed with prA as a ladder, and sizes of mRNA1 products, such as B5 (77 nt), B4 (71 nt) and B1 (47 nt) are indicated. Only the *dom34* lane is shown. See Supplementary Fig. 6a for the sequence probed by prH. The 5S rRNA served as a loading control. Total RNA from WT cells without $(CGA)_4$ -mRNA expression served as a control, noted C. A non-specific band is indicated by an asterisk. **c** Xrn1 treatment in vitro of total RNA from *dom34* or *dom34/ski2* mutant cells and northern blot using probe prH. The 5.8S rRNA is a positive control of Xrn1 treatment. **d** PCR products obtained from 3'-RACE (see also Fig. 3c). Prior to PCR, cDNAs were produced from cells expressing $(CGA)_4$ -mRNA. Total RNA from cells without $(CGA)_4$ -mRNA expression served as a control. **e** Sequences obtained after 3'-RACE performed in **d** on *ski2/DOM34* total RNA. Sequence distribution is given in percentage. **f** Primer extension experiments using probe prJ to determine the 5'-end of RNAs. Xrn1-specific arrests are indicated by arrowheads. **g** Positioning of 3'-ends detected by 3'-RACE on $(CGA)_4$ -mRNA from *ski2/DOM34* cells (magenta arrowhead). Arrowhead sizes are proportional to the relative number of sequences obtained. Three cleavage clusters, C1, C2 and C3 were defined (see Supplementary Fig. 6d). Xrn1 arrests deduced from **f** are indicated by black arrowhead with sizes proportional to the intensity of reverse stops observed in **f**. **h** Schematic view of the ribosome positioning on $(CGA)_4$ -mRNA deduced from Xrn1 arrests combined with the positioning of endonucleolytic cleavages provided by 3'-RACE. Source data are provided as a Source Data file.

nts, respectively), indicating that they do not occur to any significant level. The major ~65-bp RT-PCR product corresponded perfectly to an RNA cleaved 71nt upstream of the 3'-extremity of mRNA1, suggesting this is the primary site of NGD cleavage. This also suggests that the particular conformation of disomes on

these mRNAs is incompatible with an NGD endonuclease activity cutting upstream of the ribosome P-site. The ability to induce this precise NGD cleavage appears thus to be a normal property of stalled ribosomes, with disomes (and monosomes) being exceptions.

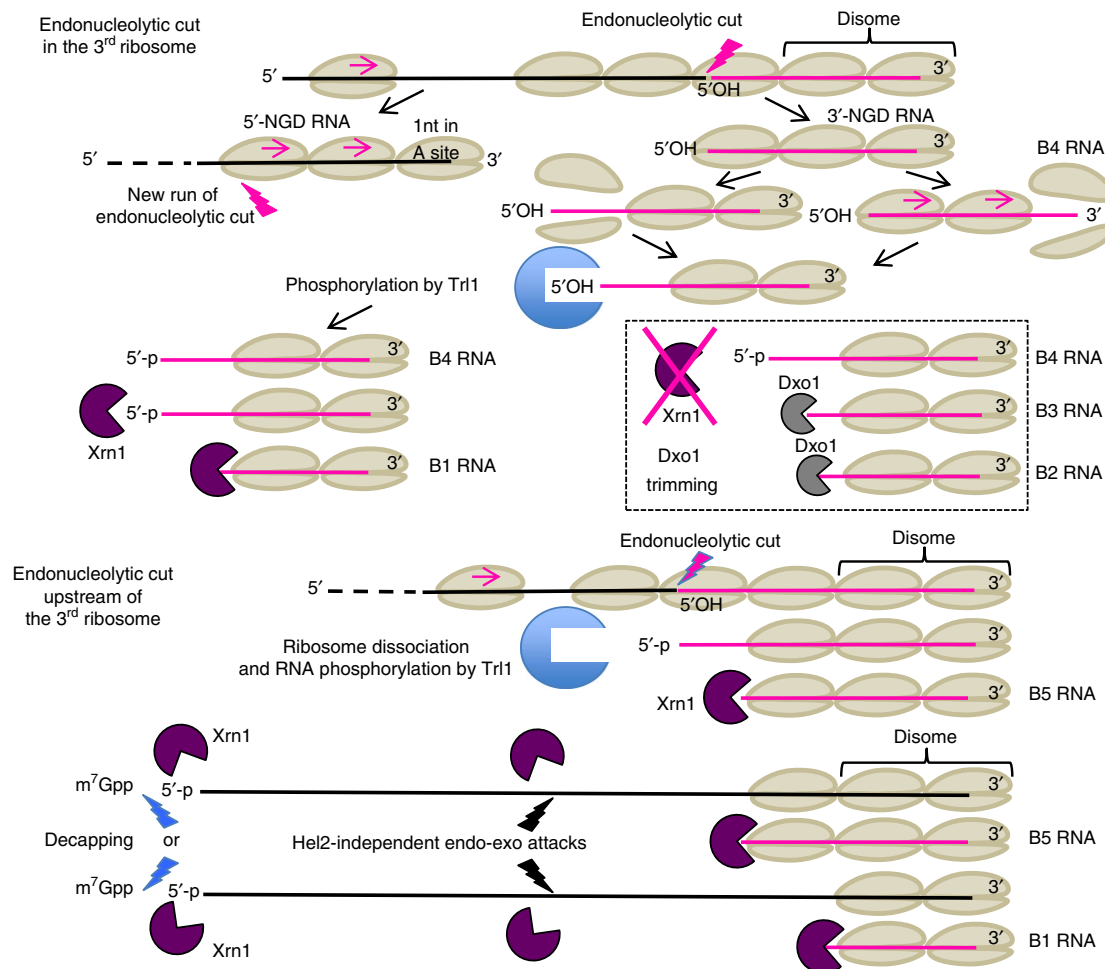


Fig. 7 Model of No-Go decay pathway involving Trl1 kinase and 5'-3' exonucleases. Top of figure, the third ribosome is represented as competent for NGD endonuclease activation. We propose that the two first stalled ribosomes are not properly conformed to trigger the endonucleolytic process. NGD endonuclease cleavage (lightning flash) occurs 8 nts upstream of the first P-site residue, within the mRNA exit tunnel of the ribosome. Upstream ribosomes covering the resulting 5'-NGD fragments can advance and stall on the new 3'-end with 1 nt in the ribosomal A-site. Colliding ribosomes on this new RNA fragment can induce a novel NGD endonuclease activation. On 3'-NGD RNAs, like B4 RNAs, the NGD-competent ribosome dissociates and facilitates access of Trl1 RNA kinase to the 5'-hydroxylated 3'-NGD RNA, but we cannot exclude that the leading ribosome dissociates and upstream ribosomes run to form a new disome with 5'-protruding RNA. Once the RNA is 5'-phosphorylated, the processive 5'-3' exonucleolytic activity of Xrn1 can degrade and produce B1 RNA. Alternatively, upon Xrn1 inactivation, 5'-3' exonucleolytic digestion of this RNA by Dxo1 can occur and produce trimmed RNAs, such as B3 and B2 RNAs. Middle of figure, upstream of the 3rd ribosome, ribosomes are also competent for NGD endonuclease activation. Here, the endonucleolytic cleavage occurs in the 4th ribosome and B5 RNAs can derive from such RNAs after phosphorylation and 5'-3' digestion. Bottom of figure, alternative pathways are proposed: B1 and B5 RNA production could be initiated by decapping or via Hel2-independent uncharacterized endo/exonucleolytic attacks.

We considered the possibility that the *dom34* mutation may exaggerate the ribosome stalling and allow cleavage beyond what would naturally be observed. As discussed in the section Introduction, the analysis of NGD RNA fragments is facilitated by the *dom34* mutation and is crucial for RNA stabilization when analysing truncated mRNAs by northern blotting experiments^{5,20}. In the presence of Dom34, and more efficient ribosome dissociation, the exosome would certainly be more actively involved once the first endonucleolytic cleavage event has occurred^{5,20}. Importantly, however, our 3'-RACE experiments confirmed the existence of 5'-NGD products with 3'-ends matching the 5'-extremity of the 3'-NGD B4 RNA in cells containing Dom34 (Fig. 3c, d). Thus, NGD endonucleolytic cleavage does not occur randomly upstream of the ribosomal stall site and is not an artefact of *dom34* genetic context.

These observations were used to map endonucleolytic cleavages that occur on a second NGD-target mRNA containing rare

codons, also in a *DOM34* genetic context. Endonucleolytic cleavages occurred 71nts upstream of the first residue in the leading ribosome A-site, in the region potentially covered by the third ribosome. Therefore, mRNAs containing rare codons are processed similar to truncated RNAs, although cleavage accuracy is slightly affected, correlating with specific Xrn1 arrests (Fig. 6f) that might be explained by a particular conformation of the first stalled ribosome²⁹.

It has been recently reported that Cue2 is the endonuclease that cleaves NGD/NSD targeted RNAs^{36,37}. Its action has been proposed to occur in the ribosome A site and therefore deviates significantly from our observations. We do not have a good explanation for this difference. However, previous experiments with the naturally occurring truncated HAC1 mRNA are consistent with our mapping of the endonucleolytic cleavage site²⁰. The HAC1 intron is known to be excised by Ire1, but RNA ligation can be incomplete and lead to a truncated but translated

mRNA^{38,39}. Green and colleagues showed by ribosome-profiling analysis that ribosomes stall at the 3'-end of the first exon of the HAC1 mRNA, leading to an endonucleolytic cleavage ~70 nt upstream from the 3'-end⁹. Consistent with this observation, our data suggests that the NGD endonuclease cleaves 71 nt upstream of the 3'-end of the truncated mRNA1 (B4 RNAs, Fig. 1g). We also showed that the NGD endonuclease cleaves mRNA1 in the +1 reading frame. As a consequence, upstream ribosomes run forward on the 5'-NGD mRNA and stall with 1 nt in the A-site (Figs. 1g and 7). This is in agreement with ribosome-profiling analysis reporting the predominance of short RNAs having one 3'-nucleotide in the ribosome A site^{20,36}.

We showed that the Trl1 kinase plays a role in NGD, and we propose that the resistance of the B4 3'-NGD RNA fragments to Xrn1 attacks in vitro and in vivo (Fig. 3a and Supplementary Figs. 1b and 3a) is a direct consequence of the 3rd ribosome preventing access to Trl1, with dissociation of this ribosome triggering the 5'-phosphorylation of the B4 RNA (Fig. 7). It is also possible that the leading ribosome dissociates, and that upstream ribosomes run forward to form a new disome with a 5'-protruding RNA (Fig. 7). Once the RNA is 5'-phosphorylated, the processive 5'-3' exonucleolytic activity of Xrn1 can degrade to produce the disome protected B1 RNA (Fig. 7). The fact that RNAs longer than B5, which accumulate in the *trl1* mutant (Fig. 5a), are Xrn1-resistant (Fig. 5c and Supplementary Fig. 5) coupled with the absence of the B5 RNA upon Xrn1 inactivation (Fig. 1b-d) lead us to propose that the B5 RNA originates from 5'-OH RNAs cleaved within ribosomes upstream of the 3rd ribosome, are phosphorylated by Trl1 and are digested by Xrn1 until it bumps into downstream ribosomes (Fig. 7). A portion of the B1 species (Fig. 5a and Supplementary Fig. 5a) is detected upon Trl1 inactivation, however. Therefore, 5'-phosphorylation of 5'-hydroxylated B4 RNAs only accounts for a portion of B1 RNA production. In agreement, the *hel2* mutation abolishes B4 RNA detection without impacting B1 and B5 RNA levels (Supplementary Fig. 3b). Mutations can thus reveal the existence of alternative pathways. In this regard, we learned that the inactivation of Xrn1 can lead to a Dxo1 trimming and production of B2 and B3 RNAs (Fig. 7). We cannot exclude the possibility that a portion of the B1 and B5 RNAs derive from alternative pathways, such as the canonical 5'-3' decay pathway (i.e., decapping and Xrn1 5'-3' digestion)²⁴ or an uncharacterized endo and/or exonucleolytic decay pathway (Fig. 7). Lower levels of NGD RNAs in a *dcp2* mutant (Fig. 1b, c) do not contradict a decapping requirement in some of their production, but the poor growth of *dcp2* mutant cells prevents us from drawing further conclusions. The potential existence of alternative pathways does not overshadow the strong impact of the *trl1* mutant on NGD RNA production (Fig. 5).

We show that the NGD pathway produces RNAs bearing a 5'-hydroxyl group (Figs. 3a, 5 and 7). 5'-hydroxyl and 2'-3' cyclic phosphate 3' extremities are typically generated by metal-independent endoribonucleolytic reactions⁴⁰. We also show that the Trl1 kinase phosphorylates these 3'-NGD fragments to allow degradation by 5'-3' exoribonucleases. Thus, in addition to its role in tRNA splicing and in phosphorylation of 5'-hydroxylated exon of the HAC1 mRNA³⁴, Trl1 is an important player in NGD pathway. This study also provides mechanistic insights that will help to go further in the comprehension of mRNA surveillance pathways in connection to NGD.

Methods

Yeast media, plasmids, strains, and oligonucleotides. The media, strains of *S. cerevisiae*, oligonucleotides, synthesized DNAs and plasmids used in this study are described in the Supplementary Methods and Supplementary Tables 1, 2, 3 and 4, respectively.

Northern blot analysis. 8 OD_{600nm} of exponentially growing cells were collected by centrifugation. RNA was extracted by adding on cell pellet 500 μ l of buffer AE (50 mM Na acetate [pH 5.3], 10 mM EDTA), vortexing, and adding 500 μ l of phenol previously equilibrated in buffer AE. After vortexing, the tubes were incubated at 65 °C for 4 min and then frozen in a dry ice-ethanol mix, followed by a 15-min centrifugation at room temperature. A second extraction with 500 μ l of phenol-Tris-EDTA-chloroform was performed. RNA from 360 μ l of supernatant was precipitated with 40 μ l of 3 M Na acetate (pH 5.3) and 2.5 volumes of ethanol and centrifuged at 4 °C for 30 min. The pellet was washed in 80% ethanol, dried at room temperature and resuspended in water. After electrophoresis, RNA was blotted onto a Hybond-N + membrane (Amersham) and hybridization to end-labelled oligodeoxynucleotide probes was carried out at 42 °C overnight in Roti-Quick solution (Carl-roth). The Hybond-N + membrane was washed successively at 42 °C in 5 \times SSC-0.1% SDS and twice in 1 \times SSC-0.1% SDS. Blots were exposed to PhosphorImager screens, scanned using a Typhoon FLA 9500 (Fuji), and quantified with ImageJ software.

Gel electrophoresis for separation of RNA molecules. Total RNA was resolved by 8% TBE-urea polyacrylamide or 1.4% TBE-Agarose gels, and to dissociate 5'-hydroxylated from 5'-phosphorylated RNAs, total RNA was resolved by 12% TBE-urea polyacrylamide gels. All gels were followed by northern blot analysis.

In vitro RNA digestion. RNA digestion of 20 OD_{260nm} of cell extracts were performed by using 1 unit of Xrn1 (Biolabs) in NEB buffer 3 at 25 °C during 30 min unless otherwise indicated. NEB Buffer 3 was replaced by T4 PNK buffer (NEB) in kinase assays in the presence or absence of Xrn1 (Figs. 3a and 5d). For RNase I treatment of cell extracts, 20 OD_{260nm} of extracts (prepared without heparin) were incubated with 0.5, 1, or 2 μ l of RNase I (Invitrogen, 100 units/ μ l) 30 min at 25 °C. For total RNA treatment, 5 μ g of RNA were digested 30 min at 25 °C. All RNase treatments were followed by RNA extraction and northern blot analysis as described above.

Polysome analysis. Yeast cells were grown exponentially to 0.8 OD₆₀₀ at 28 °C and the 200 ml cell culture was quickly cooled in ice water and then centrifuged and washed in 20 ml of buffer A containing 10 mM Tris pH 7.4, 100 mM NaCl and 30 mM MgCl₂, and 0.5 mg/ml heparin. Heparin was only omitted for RNase I treatment²⁴. Cycloheximide was not used to prevent any drug-induced ribosome positioning. The cell pellet was resuspended in 0.6 ml of buffer A. A 1.4 g amount of glass beads was added, and cell lysis was performed by bead beating twice for 30 s each time (with intermittent cooling). After lysis, the cell extract was clarified for 5 min at full speed in a microcentrifuge. The equivalent of 20 OD_{260nm} units of cell extract (80 μ g of total RNA) was then layered onto linear 10–50% sucrose density gradients. Sucrose gradients (in 10 mM Tris-HCl [pH 7.4], 70 mM ammonium acetate, 30 mM MgCl₂) were prepared in 12 \times 89 mm polyallomer tubes (Beckman Coulter). Polysome profiles were generated by continuous absorbance measurement at 254 nm using the Isco fraction collector. Gradients were collected in 20 fractions and processed for northern blotting as described above.

Primer extension. Radiolabelled primers (primers prA and prE for mRNA1, and primer prJ for (CGA)₄-mRNA) were used and Maxima H Minus reverse transcriptase (ThermoFisher) was used to synthesize a single-stranded DNA toward the 5'-end of the RNA. The size of the labelled single-stranded DNA was determined relative to a sequencing ladder (ThermoFisher Sequenase sequencing kit) on 5% TBE-urea polyacrylamide gel. Oligonucleotides were radio-labelled with [γ -32P] ATP with the T4 polynucleotide kinase (NEB).

3'-end RNA mapping. Mapping was performed according to the 3'-RNA ligase-mediated RACE method³¹ with minor modifications: Total RNA preparations were first 3'-dephosphorylated using T4 PNK for 1 h at 37 °C without ATP and pre-adenylated linker (Universal miRNA cloning linker, NEB) ligation was performed during 4 h at 22 °C in the presence of truncated RNA ligase 2 (NEB)³⁰. Reverse transcriptase reactions were performed using primer prE complementary to the linker sequence. PCR primer prF specific to mRNA1, or primer prK specific to (CGA)₄-mRNA, were used with primer prE in PCR reactions (Supplementary Figs. 3a and 6c). PCR products were purified, cloned into Zero Blunt TOPO PCR Cloning vector (Invitrogen), transformed and plasmids sequenced.

Reporting Summary. Further information on research design is available in the Nature Research Reporting Summary linked to this Article.

Data availability

A Reporting Summary for this Article is available as a Supplementary Information file. The authors declare that all data supporting the findings of this study are available within the Article and its Supplementary Information files or from the corresponding author upon reasonable request. The source data underlying Figs. 1b-f, 2a, b, 3a, c, 4b, c, 5a-d and 6b-d, f and Supplementary Figs. 1b, d-i, 2a-c, 3a, b, 5 and 6b, e are provided as a Source Data file in the Supplementary Information and at FigShare with DOI information (0.6084/m9.figshare.11317613).

Received: 8 November 2018; Accepted: 11 December 2019;

Published online: 08 January 2020

References

- Doma, M. K. & Parker, R. Endonucleolytic cleavage of eukaryotic mRNAs with stalls in translation elongation. *Nature* **440**, 561–564 (2006).
- Passos, D. O. et al. Analysis of Dom34 and its function in No-Go Decay. *Mol. Biol. Cell* **20**, 3025–3032 (2009).
- Chen, L. et al. Structure of the Dom34–Hbs1 complex and implications for No-Go Decay. *Nat. Struct. Mol. Biol.* **17**, 1233–1240 (2010).
- Letzring, D. P., Dean, K. M. & Grayhack, E. J. Control of translation efficiency in yeast by codon–anticodon interactions. *RNA* **16**, 2516–2528 (2010).
- Tsuboi, T. et al. Dom34:hbs1 plays a general role in quality-control systems by dissociation of a stalled ribosome at the 3' end of aberrant mRNA. *Mol. Cell* **46**, 518–529 (2012).
- Simms, C. L., Hudson, B. H., Mosior, J. W., Rangwala, A. S. & Zaher, H. S. An active role for the ribosome in determining the fate of oxidized mRNA. *Cell Rep.* **9**, 1256–1264 (2014).
- Sinturel, F. et al. Cytoplasmic control of sense–antisense mRNA pairs. *Cell Rep.* **12**, 1853–1864 (2015).
- Simms, C. L., Thomas, E. N. & Zaher, H. S. Ribosome-based quality control of mRNA and nascent peptides. *RNA* **8**, e1366 (2017).
- Guydosh, N. R. & Green, R. Translation of poly(A) tails leads to precise mRNA cleavage. *RNA* **23**, 749–761 (2017).
- Frischmeyer, P. A. et al. An mRNA surveillance mechanism that eliminates transcripts lacking termination codons. *Science* **295**, 2258–2261 (2002).
- van Hoof, A., Frischmeyer, P. A., Dietz, H. C. & Parker, R. Exosome-mediated recognition and degradation of mRNAs lacking a termination codon. *Science* **295**, 2262–2264 (2002).
- Kuroha, K. et al. Receptor for activated C kinase 1 stimulates nascent polypeptide-dependent translation arrest. *EMBO Rep.* **11**, 956–961 (2010).
- Brandman, O. et al. A ribosome-bound quality control complex triggers degradation of nascent peptides and signals translation stress. *Cell* **151**, 1042–1054 (2012).
- Defenouillere, Q. et al. Cdc48-associated complex bound to 60S particles is required for the clearance of aberrant translation products. *Proc. Natl Acad. Sci. USA* **110**, 5046–5051 (2013).
- Shen, P. S. et al. Protein synthesis. Rqc2p and 60S ribosomal subunits mediate mRNA-independent elongation of nascent chains. *Science* **347**, 75–78 (2015).
- Johnson, A. W. & Kolodner, R. D. Synthetic lethality of sep1 (xrn1) ski2 and sep1 (xrn1) ski3 mutants of *Saccharomyces cerevisiae* is independent of killer virus and suggests a general role for these genes in translation control. *Mol. Cell. Biol.* **15**, 2719–2727 (1995).
- Shoemaker, C. J., Eyler, D. E. & Green, R. Dom34:Hbs1 promotes subunit dissociation and peptidyl-tRNA drop-off to initiate no-go decay. *Science* **330**, 369–372 (2010).
- Meaux, S. & Van Hoof, A. Yeast transcripts cleaved by an internal ribozyme provide new insight into the role of the cap and poly(A) tail in translation and mRNA decay. *RNA* **12**, 1323–1337 (2006).
- Guydosh, N. R., Kimmig, P., Walter, P. & Green, R. Regulated Ire1-dependent mRNA decay requires no-go mRNA degradation to maintain endoplasmic reticulum homeostasis in *S. pombe*. *eLife* **6**, e29216 (2017).
- Guydosh, N. R. & Green, R. Dom34 rescues ribosomes in 3' untranslated regions. *Cell* **156**, 950–962 (2014).
- Wu, J. & Hopper, A. K. Healing for destruction: tRNA intron degradation in yeast is a two-step cytoplasmic process catalyzed by tRNA ligase Rlg1 and 5'-to-3' exonuclease Xrn1. *Genes Dev.* **28**, 1556–1561 (2014).
- Chang, J. H. et al. Dxo1 is a new type of eukaryotic enzyme with both decapping and 5'-3' exoribonuclease activity. *Nat. Struct. Mol. Biol.* **19**, 1011–1017 (2012).
- Parker, R. RNA degradation in *Saccharomyces cerevisiae*. *Genetics* **191**, 671–702 (2012).
- Hu, W., Sweet, T. J., Chamnongpol, S., Baker, K. E. & Collier, J. Co-translational mRNA decay in *Saccharomyces cerevisiae*. *Nature* **461**, 225–229 (2009).
- Ingolia, N. T., Ghaemmaghami, S., Newman, J. R. & Weissman, J. S. Genome-wide analysis in vivo of translation with nucleotide resolution using ribosome profiling. *Science* **324**, 218–223 (2009).
- Pelechano, V., Wei, W. & Steinmetz, L. M. Widespread co-translational RNA decay reveals ribosome dynamics. *Cell* **161**, 1400–1412 (2015).
- Simms, C. L., Yan, L. L. & Zaher, H. S. Ribosome collision is critical for quality control during No-Go Decay. *Mol. Cell* **68**, 361–373 (2017).
- Nagarajan, V. K., Jones, C. I., Newbury, S. F. & Green, P. J. XRN 5'->3' exoribonucleases: structure, mechanisms and functions. *Biochim. Biophys. Acta* **1829**, 590–603 (2013).
- Ikeuchi, K. et al. Collided ribosomes form a unique structural interface to induce Hel2-driven quality control pathways. *EMBO J.* **38**, e100276 (2019).
- McGlinchy, N. J. & Ingolia, N. T. Transcriptome-wide measurement of translation by ribosome profiling. *Methods* **126**, 112–129 (2017).
- Adkar-Purushothama, C. R., Bru, P. & Perreault, J. P. 3' RNA ligase mediated rapid amplification of cDNA ends for validating viroid induced cleavage at the 3' extremity of the host mRNA. *J. Virol. Methods* **250**, 29–33 (2017).
- Phizicky, E. M., Consaul, S. A., Nehrke, K. W. & Abelson, J. Yeast tRNA ligase mutants are nonviable and accumulate tRNA splicing intermediates. *J. Biol. Chem.* **267**, 4577–4582 (1992).
- Cherry, P. D., White, L. K., York, K. & Hesselberth, J. R. Genetic bypass of essential RNA repair enzymes in budding yeast. *RNA* **24**, 313–323 (2018).
- Cherry, P. D., Peach, S. E. & Hesselberth, J. R. Multiple decay events target HAC1 mRNA during splicing to regulate the unfolded protein response. *eLife* **8**, e42262 (2019).
- Chen, H. & Xiong, L. The bifunctional abiotic stress signalling regulator and endogenous RNA silencing suppressor FIERY1 is required for lateral root formation. *Plant Cell Environ.* **33**, 2180–2190 (2010).
- D'Orazio, K. N. et al. The endonuclease Cue2 cleaves mRNAs at stalled ribosomes during No Go Decay. *eLife* **8**, e49117 (2019).
- Glover, M. L. et al. NONU-1 encodes a conserved endonuclease required for mRNA translation surveillance. Preprint at <https://doi.org/10.1101/674358> (2019).
- Cox, J. S. & Walter, P. A novel mechanism for regulating activity of a transcription factor that controls the unfolded protein response. *Cell* **87**, 391–404 (1996).
- Harigaya, Y. & Parker, R. Global analysis of mRNA decay intermediates in *Saccharomyces cerevisiae*. *Proc. Natl Acad. Sci. USA* **109**, 11764–11769 (2012).
- Gonzalez, T. N., Sidrauski, C., Dorfler, S. & Walter, P. Mechanism of non-spliceosomal mRNA splicing in the unfolded protein response pathway. *EMBO J.* **18**, 3119–3132 (1999).

Acknowledgements

This work has been supported by AAP Emergence Sorbonne Université, SU-16-R-EMR-03 and by the “Initiative d’Excellence” program from the French State grant “DYNAMO”, ANR-11-LABX-0011-01. S.C. was a recipient of fellowship from the Ministère pour la Recherche et la Technologie (MNRT). A.N. was supported by a doctoral grant from “DYNAMO”, ANR-11-LABX-0011-01. We thank Jay Hesselberth for providing *trl1* mutant and Jeff Collier for the *dep2Δ* mutant. We thank Ciaran Condon, Josette Banroques and Kyle Tanner for technical assistance. We thank Ciaran Condon for comments on the manuscript and constructive discussions. The first two authors are listed in chronological order of contribution.

Author contributions

A.N., S.C., R.S.-F., J.H., C.T. and L.B. designed, performed and analysed data. L.B. wrote the manuscript.

Competing interests

The authors declare no competing interests.

Additional information

Supplementary information is available for this paper at <https://doi.org/10.1038/s41467-019-13991-9>.

Correspondence and requests for materials should be addressed to L.B.

Reprints and permission information is available at <http://www.nature.com/reprints>

Publisher's note Springer Nature remains neutral with regard to jurisdictional claims in published maps and institutional affiliations.



Open Access This article is licensed under a Creative Commons Attribution 4.0 International License, which permits use, sharing, adaptation, distribution and reproduction in any medium or format, as long as you give appropriate credit to the original author(s) and the source, provide a link to the Creative Commons license, and indicate if changes were made. The images or other third party material in this article are included in the article's Creative Commons license, unless indicated otherwise in a credit line to the material. If material is not included in the article's Creative Commons license and your intended use is not permitted by statutory regulation or exceeds the permitted use, you will need to obtain permission directly from the copyright holder. To view a copy of this license, visit <http://creativecommons.org/licenses/by/4.0/>.

© The Author(s) 2020